

The Effects of Microvoid Defects on MWIR HgCdTe-Based Diodes

C.A. BILLMAN,^{1,3} L.A. ALMEIDA,¹ P. SMITH,¹ J.M. ARIAS,¹ A. CHEN,² D. LEE,² and E.C. PIQUETTE²

1.—U.S. Army, RDECOM CERDEC, NVESD, Fort Belvoir, VA, USA. 2.—Teledyne Imaging Sensors, Camarillo, CA, USA. 3.—e-mail: info@nvl.army.mil

The effects of microvoid defects on the performance of mid-wavelength infrared (MWIR) HgCdTe-based diodes were examined. Molecular beam epitaxy (MBE) was utilized to deposit indium-doped, $Hg_{0.68}Cd_{0.32}Te$ on 2 cm × 3 cm, (211)B-oriented, bulk $Cd_{0.96}Zn_{0.04}Te$ substrates. These epilayers generally exhibited state-of-the-art material properties with a notable exception: high and nonuniform microvoid defect densities (mid 10^4 cm^{-2} to low 10^6 cm^{-2}). Diodes were fabricated by ion implantation of arsenic to form planar $p-n$ junctions. Dark current–voltage ($I-V$) curves were measured and analyzed as a function of operating temperature. There was an inverse correlation between wafer-level microvoid defect density and device operability. On each wafer, devices with the smallest implants exhibited higher operability than devices with larger implants. By removal of pad metal and examination of defects within each implant area, it was found that the presence of one or more microvoids within the junction usually caused tunneling or other high-current mechanisms. Diodes free from microvoids exhibited diffusion-limited behavior down to 150 K, the test set limit.

Key words: HgCdTe, defects, microvoid, infrared detector, dark current

INTRODUCTION

A prevalent defect in molecular beam epitaxial HgCdTe is the microvoid defect. Commonly observed on (211)B-oriented epilayers, they have also been observed on other, similar orientations. They have not been described on (001) or similar surfaces, where pyramidal hillock defects are the dominant defect type. Microvoid and similar defects have been described in several previous studies,^{1–7} using a variety of distinct terms including void-hillock complex,⁵ triangle defects,⁶ etc. These previous studies, while using varying terminology and characterization techniques, seem to describe a single class of defects with the following characteristics:

The defect is small, defined approximately by a lateral extent smaller than the thickness of the epilayer. It is this characteristic that led to the

name “microvoid” as distinct from the earlier classified “void” defect.⁸

The defect is composed of a polycrystalline core that lies slightly below the surface of the epilayer and an elevated ridge that runs along [011]. The structure of the microvoid is again distinct from the void, which is typically deeper, and may or may not be filled with polycrystalline material.^{1,2}

Often, but not always, microvoids are associated with clusters, or nesting of dislocations, as revealed by decoration etching, whereas void defects are not typically associated with such clusters.^{5,7}

There is no consensus on the cause of these defects, with various explanations having been offered, including Hg-rich growth conditions,^{1,2} temporal variations in growth conditions,⁵ and substrate-originated defects.^{3,4} This work does not address the cause of these defects but describes the effects of these defects on infrared photodiodes fabricated using HgCdTe containing various densities of such defects.

The effects of void defects were described in the early days of MBE development;⁸ specifically, a void defect coinciding with a metal contact would result in a short of the junction and device failure. Only a few studies on the effects of microvoids on device performance have been published. In both cases, a one-to-one correlation between microvoid defects and device performance was difficult to discern. Varesi et al.⁶ performed failure analysis of focal-plane arrays and concluded that about half of microvoids had deleterious effects. Wijewaurnaursaurya et al.⁷ classified three distinct types of defects and carried out failure analysis on individual long-wavelength infrared (LWIR) detectors using R_0A as the primary figure of merit; this study also concluded that not all microdefects caused diode failure. The present work attempts similar failure analysis on MWIR diodes to study the effects of microvoids on diode performance, but utilizing a more careful analysis of current-voltage characteristics, particularly focusing on the more demanding conditions of low temperature and high reverse bias.

EXPERIMENTAL PROCEDURES

$Hg_{0.68}Cd_{0.32}Te$ epilayers were deposited on 2 cm × 3 cm, (211)B-oriented, $Cd_{0.96}Zn_{0.04}Te$ substrates at Night Vision and Electronic Sensors Directorate (NVESD). These epilayers were characterized by a variety of techniques, including Fourier-transform infrared (FTIR) transmission, Hall measurement, Nomarski microscopy, scanning electron microscopy (SEM), and defect decoration etching. The outstanding feature of these epilayers was a high and nonuniform density of microvoid defects. While the exact cause of the observed microvoid defects is not known, it is believed they are due to one of the mechanisms mentioned above and more fully discussed in Ref. 1.

While three such epilayers were chosen for subsequent device fabrication, detailed analysis of the device results from two such wafers are presented herein due to their well-matched cutoff wavelengths (Table I). Diodes were fabricated using a standard, double-layer, planar heterostructure (DLPH) architecture, which employed ion implantation of arsenic to form planar $p-n$ junctions. Each wafer

was printed with a single process evaluation chip (PEC), consisting of discrete devices of various sizes and two focal-plane arrays (FPA), whose format was 640 × 512 on a 15 μm pitch. The PEC diodes that formed the bulk of this study were 16-μm-, 32-μm-, 64-μm-, and 125-μm-diameter circular implants and 11 μm × 11 μm square-shaped implants, which mimicked the FPA device architecture. Based on PEC device results, one FPA was selected for hybridization and testing. The devices of the three PECs were thoroughly characterized, at both Teledyne Imaging Sensors (TIS) and NVESD, with good agreement between the two test sets. Dark current-voltage ($I-V$) curves were measured as a function of operating temperature (300 K to 77 K). Spectral response and quantum efficiency (QE) were measured at TIS. A simple analysis of the PEC results formed the basis of this work: the correlation of the prevalence of microvoid defects with device performance degradation, primarily evaluated by dark current density. Diode results from a control sample with lower microvoid defect density and with similar cutoff wavelength (grown and processed at TIS) were used for comparison.

Additionally, the PECs were stripped of their pad metal in order to ascertain definitively the presence of microvoids in and around the implant area of individual diodes and to evaluate the impact of such microvoids on diode performance. Nomarski micrographs were taken of each implant area, and microvoids within and near the implant were counted. In some cases, SEM imagery was used when discernment of a microvoid was unclear in the Nomarski micrograph.

RESULTS

Material Characteristics

The wafers chosen for device fabrication were selected from a set of about 40 growth runs. These growth runs resulted in epilayers of largely similar characteristics, which are summarized here. FTIR transmission data demonstrated good control of growth rate and x -value. This control has been enabled by the use of *in situ* spectroscopic ellipsometry. The target, FTIR-determined x -value of 0.325 was routinely met with an accuracy of ~0.003. The typical growth rate determined by FTIR was ~2.5 μm h⁻¹. Hall measurements at 77 K indicated n -type conduction with carrier concentrations of ~2 × 10¹⁵ cm⁻³ and mobilities of ~30,000 cm² V⁻¹ s⁻¹. Nomarski microscopy revealed microvoid defects as the prevalent defect. The microvoids were found to be nonuniformly distributed across a wafer at elevated densities (~10⁴ cm⁻² to 10⁶ cm⁻²). Table I summarizes microvoid densities measured on the wafers chosen for subsequent device processing and on the control sample. The microvoid density that was measured directly on the processed PEC (near wafer's edge) is shown separately from the density measured in the "typical best" area (generally near

Table I. Material characteristics of processed wafers

| | Thickness (μm) | 150-K Cutoff (μm) | Microvoid Defect Density (cm ⁻²) | |
|----------|-------------------|-------------------------|---|----------------------|
| | | | Measured on PEC | Typical Best Area |
| Sample 1 | 7.8 | 4.26 | 2.0 × 10 ⁵ | 6 × 10 ⁴ |
| Sample 2 | 7.5 | 4.24 | 1.5 × 10 ⁶ | 4 × 10 ⁵ |
| Sample 3 | 7.1 | 4.50 | 8.2 × 10 ⁴ | 3 × 10 ⁴ |
| Control | 9.8 | 4.20 | 6.7 × 10 ³ | 2 × 10 ³ |

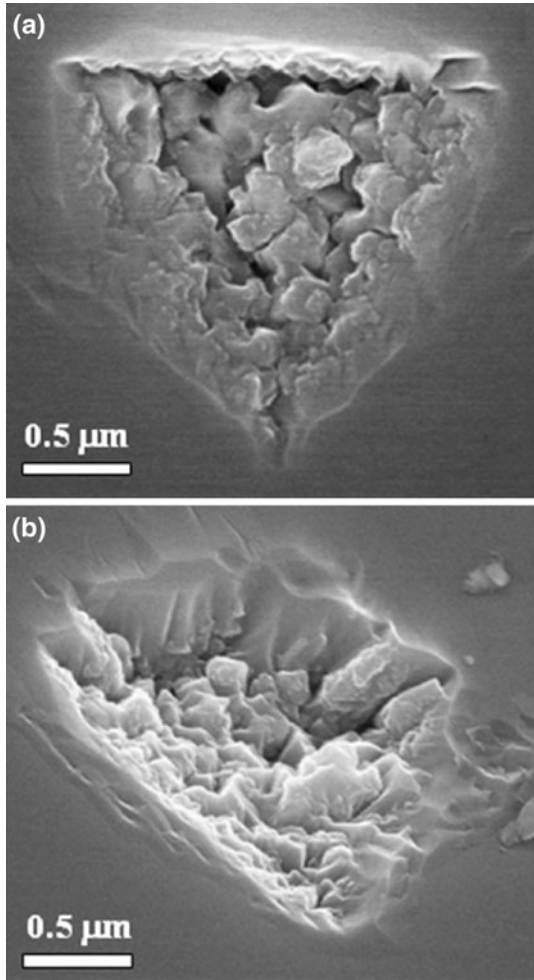


Fig. 1. SEM images of typical microvoid defects (a) in normal view (b) at about 45° from normal.

wafer's center). Other typical surface features revealed by Nomarski microscopy were cross-hatch patterning, needle defects, and void defects. SEM images, such as those in Fig. 1, provided details of the microvoid structure and confirmed observations from previously published studies^{1,2} regarding the geometry and morphology of microvoid defects in HgTe and HgCdTe. Defect decoration etching was used to estimate the dislocation density of the epilayers. Typically, Nomarski microscopy and occasionally SEM were used to image the resulting surfaces. Typical etch pit density values were $< 5 \times 10^5 \text{ cm}^{-2}$.

Diode Characteristics

Each PEC diode from each wafer was characterized by I - V measurements from 300 K to 77 K. Below ~ 150 K the current measurements were limited by system capability. At 150 K some diodes from the high-defect-density samples exhibited diffusion-limited I - V characteristics, comparable to those of the lower-defect-density, control sample.

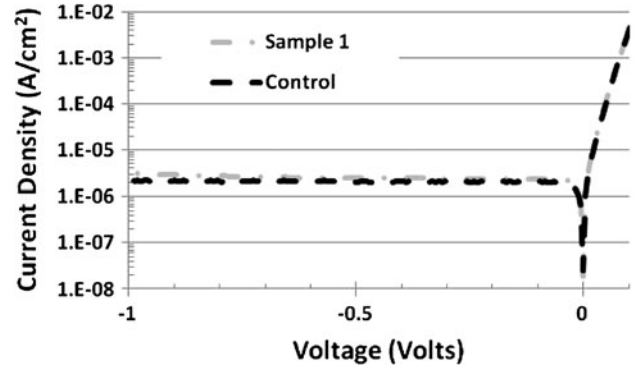


Fig. 2. I - V curves from two 32- μm circular diodes, one from sample 1 and the other from the TIS control sample. The I - V characteristics are essentially indistinguishable.

This is shown in Fig. 2, which is a plot of I - V taken at 150 K from a diode from sample 1 and from a geometrically similar diode from the control sample. This data demonstrated that very high-performance diodes could be fabricated from material with high microvoid defect density; however, high performance was not observed in all diodes. Figure 3 shows three, distinct, typically observed I - V plots taken at 300 K, 250 K, 200 K, and 150 K from three geometrically similar diodes from sample 1. Figure 3a shows I - V plots which were diffusion limited at each temperature. Figure 3b shows I - V plots characterized by increased current at larger bias voltage and at lower temperature; these characteristics indicated a tunneling mechanism. Figure 3c shows I - V plots with excessive current below about 200 K and without a strong bias dependence of the current.

Due to the variability in the diode I - V characteristics, two criteria were utilized to define operable diodes. The first criterion was that the measured current must be less than $1 \times 10^{-10} \text{ A}$ at 150 K and 50 mV reverse bias. It was found that this simple, low-current condition need not depend on current density (implant size), due to the large, lateral, diffusion lengths of these devices and due to the relatively limited range of diode sizes examined herein. The second criterion was that the current must be diffusion limited down to 150 K; this condition was quantified by comparing the optical bandgap with the activation energy derived from an Arrhenius plot of the current density, again at 50 mV reverse bias. Operable diodes were those that met both, aforementioned criteria. The operability of each size class of diodes is shown in Table II, which also shows the operability of all 12 small diodes (16- μm circular and 11 $\mu\text{m} \times 11 \mu\text{m}$ square) and of all 12 large diodes (32- μm , 64- μm , and 125- μm circular). The control sample had 100% diode operability for all diodes under test, consistent with its lower microvoid density. Samples 1 and 2 both had higher operability for smaller sized diodes compared with larger sized diodes. Sample 1

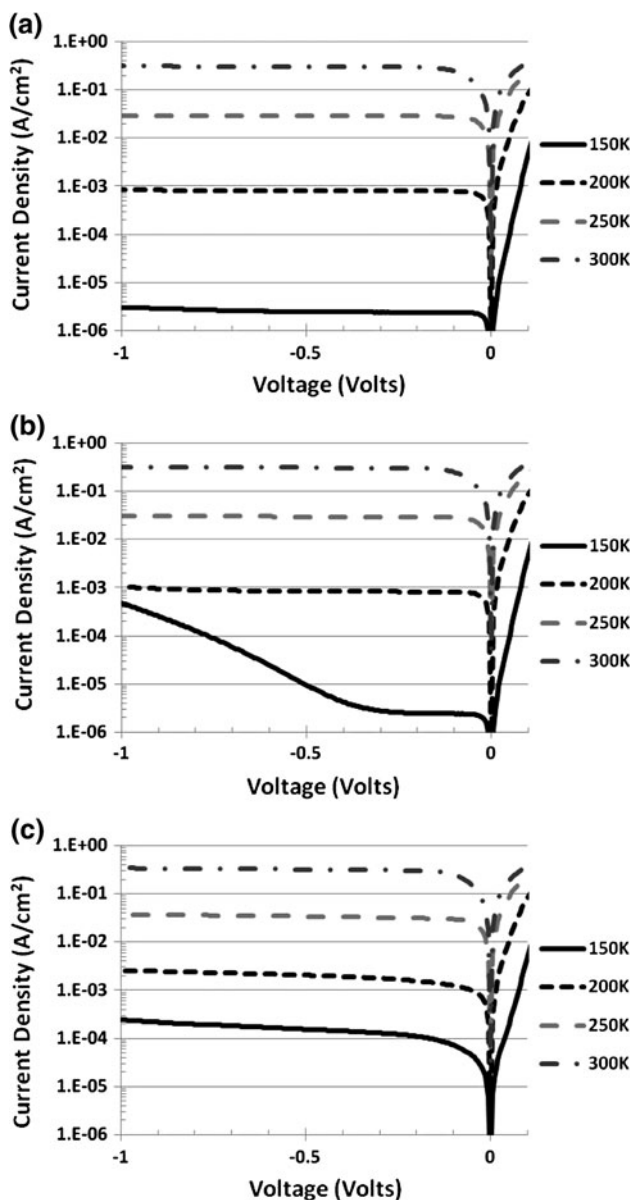


Fig. 3. I - V curves from three characteristic diodes from sample 1: (a) diffusion-limited behavior down to 150 K, (b) tunneling current mechanism evident at low temperature and high bias voltage, and (c) high current at all bias voltages.

had higher operability in each size class of diodes compared with sample 2. The operability data summarized in Table II may be qualitatively and plausibly explained by assuming that randomly distributed microvoids, residing within or near the implant area, can cause inoperable diodes, as defined above. Given this assumption, operability monotonically increases (decreases) with decreasing (increasing) implant area (microvoid density). These general trends are supported by the data of Table II.

The failure analysis, which followed metal pad stripping, further elucidated the impact of microvoids on diode performance. Each diode was examined by Nomarski microscopy for the presence or absence of microvoids. This allowed direct correlation of microvoids with I - V characteristics. Nomarski images of three similarly sized diodes are shown in Fig. 4. While the implant area could be discerned in the micrographs, a dashed line circle, coinciding with the implant area, has been added to the images of Fig. 4 for additional clarity; solid line circles surround microvoids. The image in Fig. 4a shows a diode with no microvoids within the implant area, Fig. 4b shows one microvoid within the implant, and Fig. 4c shows several microvoids within the implant.

Each diode represented in Table II was examined for the presence of microvoids within the implant to determine their impact on the I - V characteristics. Inoperable diodes were generally characterized by the presence of one or more microvoids within the implant area. Only one inoperable diode, a 64- μm circular implant from sample 1, had no apparent microvoids within its implant; this device exhibited a linear (resistor-like) I - V characteristic. On the other hand, it was found that several operable diodes contained microvoids within the implant area. Table III lists the operable diodes that had at least one microvoid within the implant and the deviation of those diodes' I - V characteristics from the control. On only two diodes was no deviation observed; in other words, the presence of a microvoid within the implant area did not measurably impact the I - V characteristics. Some diodes showed slightly higher current relative to the control and

Table II. Diode operability

| Area (10^{-6} cm^2) | Diode (#) | Sample (Microvoid Density, cm^{-2}) | | |
|---------------------------------|-----------|---|--|--|
| | | Control (6×10^3) Operability (%) | Sample 1 (2×10^5) Operability (%) | Sample 2 (1.5×10^6) Operability (%) |
| 1.21 | 15S (8) | 100 | 100 | 38 |
| 2.01 | 16C (4) | 100 | 100 | 25 |
| Small diodes | Total | 100 | 100 | 33 |
| 8.04 | 32C (4) | 100 | 75 | 50 |
| 31.2 | 64C (4) | 100 | 50 | 0 |
| 123 | 125C (4) | 100 | 50 | 0 |
| Large diodes | Total | 100 | 58 | 17 |

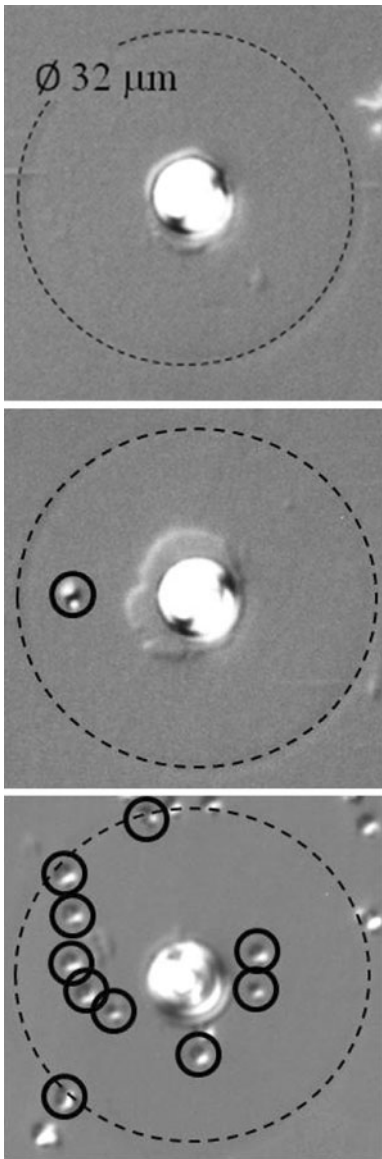


Fig. 4. Nomarski imagery of PEC diode implants after metal stripping with (a) zero, (b) one, and (c) ten microvoids (solid circles) within the 32- μm -diameter implant area (dashed circle).

relative to other diodes of the same size class. The most common impact on the I - V characteristics of microvoid-containing diodes was tunneling. Tunneling was not observed on any diodes that had zero microvoids within the implant.

Focal-Plane Array Characteristics

The fabricated FPA, with antireflection coating, was tested using a standard configuration and procedure at ~ 140 K. Its median radiometric characteristics were comparable to those of FPAs fabricated from material grown at TIS. The QE was high (mean $\sim 83\%$) and uniform (standard deviation/mean $\sim 2.8\%$). The dark current (I_D) measured on the FPA (mean $\sim 1.2 \times 10^{-7} \text{ A cm}^{-2}$) was consistent with the PEC data and historical TIS data. The

Table III. Impact of microvoids in implant area on I-V characteristics of individual diodes deemed operable

| Operable Diodes | Microvoids in Implant | Sample 1 |
|-----------------|-----------------------|-------------------------|
| 15S | 1 | No impact |
| 16C | 1 | Slightly higher current |
| 32C | 1 | Tunneling |
| 32C | 1 | Slightly higher current |
| 64C | 2 | Tunneling |
| 125C | 4 | Tunneling |

| Operable Diodes | Microvoids in Implant | Sample 2 |
|-----------------|-----------------------|-------------------------|
| 15S | 1 | No impact |
| 15S | 1 | Tunneling |
| 15S | 1 | Slightly higher current |
| 16C | 1 | Tunneling |
| 32C | 8 | Tunneling |
| 32C | 10 | Tunneling |

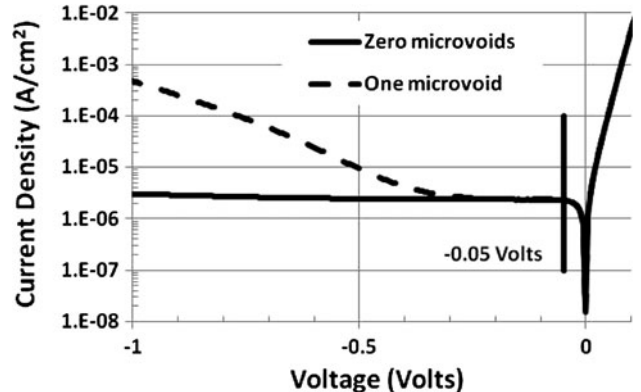


Fig. 5. I - V curves of diffusion-limited and tunneling-current-dominated diodes. The vertical line at -50 mV demonstrates that, under FPA operating conditions, diodes are virtually indistinguishable.

mean noise equivalent temperature difference (NEDT) was found to be ~ 48 mK. The operability, arbitrarily defined by the fraction of pixels with parameter values between 0.5 and $2 \times$ the mean parameter value, was 99.4%, 99.2%, and 97.6% for I_D , NEDT, and QE, respectively. The operability definition was more stringent for QE (essentially $\text{QE} > 41.5\%$), which could explain the discrepancy in its operability values compared with I_D and NEDT. The FPA was fabricated from an area on the wafer with a microvoid density of $\sim 6 \times 10^4 \text{ cm}^{-2}$, which would have led to an expected operability of $\sim 93\%$ if every microvoid within an implant area caused an inoperable pixel. The measured operabilities suggested that between 10% and 30% of microvoid defects caused inoperable pixels. This result was broadly consistent with previous studies and the analysis of PEC diodes above. Figure 5 shows I - V at 150 K for two PEC diodes: one diode without microvoids and one diode with a single

microvoid. The diode with a single microvoid shows tunneling at higher reverse bias, which was found to be the most common trait of diodes containing a microvoid. This difference between two such diodes would not be detectable within the context of FPA operation, where reverse bias was lower than where tunneling was typically observed.

CONCLUSIONS

Diffusion-limited, MWIR, photodiode performance was measured on devices fabricated from MBE $\text{Hg}_{0.68}\text{Cd}_{0.32}\text{Te}$ epilayers, deposited on $\text{Cd}_{0.96}\text{Zn}_{0.04}\text{Te}$ (211)B substrates at NVESD. These epilayers were characterized by an unusually high density and a nonuniform distribution of microvoid defects. The effects of these defects on diode performance (I - V) were studied by a simple analysis and by a more thorough failure analysis. No simple correlation was found between the presence of microvoid defects within the implant area and the effect on diode I - V characteristics. However, certain trends were established. Diffusion-limited diodes were generally free of microvoids. The presence of microvoids within the implant area generally led to higher currents in reverse bias. Occasionally these higher currents were observed at all bias values, but

more typically tunneling currents were observed at higher values of bias (>0.3 V). Tunneling currents were observed to be the most common current mechanism associated with microvoids; therefore, FPAs operating at small reverse bias are somewhat tolerant to the presence of microvoid defects with respect to dark current operability.

REFERENCES

1. E. Selvig, C.R. Tonheim, T. Lorentzen, K.O. Kongshaug, T. Skauli, and R. Haakenaasen, *J. Electron. Mater.* 37, 1444 (2008).
2. E. Selvig, C.R. Tonheim, K.O. Kongshaug, T. Skauli, T. Lorentzen, and R. Haakenaasen, *J. Vac. Sci. Technol. B* 25, 1776 (2007).
3. E.C. Piquette, M. Zandian, D.D. Edwall, and J.M. Arias, *J. Electron. Mater.* 30, 627 (2001).
4. F. Aqariden, H.D. Shih, A.M. Turner, and P.K. Liao, *J. Electron. Mater.* 30, 794 (2001).
5. D. Chandra, F. Aqariden, J. Frazier, S. Gutzler, T. Orent, and H.D. Shih, *J. Electron. Mater.* 29, 887 (2000).
6. J.B. Varesi, A.A. Buell, J.M. Peterson, R.E. Bornfreund, M.F. Vilela, W.A. Radford, and S.M. Johnson, *J. Electron. Mater.* 32, 661 (2003).
7. P.S. Wijewarnasuriya, M. Zandian, D.B. Young, J. Waldrop, D.D. Edwall, W.V. McLevige, D. Lee, J. Arias, and A.I. D'Souza, *J. Electron. Mater.* 28, 649 (1999).
8. J.M. Arias, M. Zandian, J. Bajaj, J.G. Pasko, L.O. Bubulac, S.H. Shin, and R.E. DeWames, *J. Electron. Mater.* 24, 521 (1995).